THE JOURNAL OF PHYSICAL CHEMISTRY C

Article

pubs.acs.org/JPCC

Co Polyoxometalates and a Co_3O_4 Thin Film Investigated by L-Edge X-ray Absorption Spectroscopy

Amber M. Hibberd,[†,∥] Hoang Q. Doan,[‡,∥] Elliot N. Glass,[⊥] Frank M. F. de Groot,[§] Craig L. Hill,[⊥] and Tanja Cuk*[,‡,†]

[†]Chemical Sciences Division, Lawrence Berkeley National Laboratory, 1 Cyclotron Road, Berkeley, California 94720, United States
[‡]Department of Chemistry, University of California-Berkeley, 419 Latimer Hall, Berkeley, California 94720, United States
[⊥]Department of Chemistry, Emory University, 1515, Dickey Drive, Atlanta, Georgia 30322, United States, and
[§]Department of Chemistry, Utrecht University, Universiteitsweg 99, 3584CG Utrecht, The Netherlands

Supporting Information

ABSTRACT: We have performed cobalt L-edge X-ray absorption spectroscopy (XAS) on important materials for photoactive catalysis, namely nanoscale cobalt polyoxometalates (Co POM) and a Co_3O_4 thin film. A set of Co POM analogues were studied that vary according to the position and number of cobalts within the POM structure, metal valence state, oxygen ligand coordination geometry and heteroatom identity. Ligand field multiplet calculations simulate experimental XAS spectra in well-defined model systems provided by the Co POMs and extended to a Co_3O_4 thin film, thereby characterizing atomic multiplet and ligand field effects, including the ligand field parameter, structural distortions, and electron−electron interactions for Co^{2+} and Co^{3+} ions in both O_h and T_d environments. The ligand field parameter, $10Dq$, is determined to within an accuracy of ±0.1 eV, the spectra are sensitive to small structural distortions that further split d-levels (0.16 eV), and the strength of electron−electron interactions is found to within ±5% of the atomic value. We also find that the electronic structure parameters and the XAS spectra do not vary among POMs with pronounced differences in catalytic activity, and therefore X-ray spectroscopies even more sensitive to the 3d electronic structure (such as resonant inelastic X-ray scattering (RIXS)) should be used to differentiate the more active catalysts.

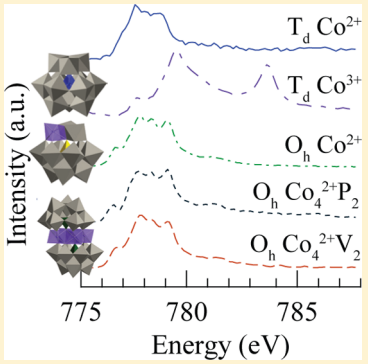

INTRODUCTION

Cobalt (Co) containing materials are used in a wide range of research fields, including spintronics, Li-ion batteries, and photoinitiated catalysis. For example, ZnO[1,2] and TiO_2[3−5] doped with small amounts of Co exhibit novel magnetic properties, such as room temperature ferromagnetism for spintronic applications and commerical applications of lithium-ion batteries routinely use Co-based electrodes.[6,7] Most importantly for this study, Co ions, such as in cobalt oxide spinel (Co_3O_4) nanoparticles,[8,9] electrodeposited Co−phosphate,[10] and Co-based polyoxometalates (POMs),[11,12] have been shown to be active catalytic centers for water oxidation. These systems have emerged as some of the most promising for harnessing solar energy through artificial photosynthesis. Since the physical and chemical properties of Co can vary widely due to the variety of valence states and bonding environments in which Co can be stable, the characterization of these catalysts by X-rays, both *in situ* and *ex situ*, has been extensive. In particular, K-edge X-ray absorption spectroscopy (XAS) that excites an electron from the 1s Co orbital to the delocalized, sp unoccupied continuum has been able to identify the approximate oxidation state and local coordination environment of the Co-phosphate catalyst prior to and during catalytic water oxidation[13] and assess the stability of the homogeneous, soluble Co-based POMs.[14,15]

While these studies are informative of the local Co environment, it is largely the 3d electrons that give rise to the detailed electronic structure. The pre-edge peak of K-edge XAS can contain information about electron excitation from the 1s to the 3d Co orbital. However, the pre-edge peak of a Co K-edge XAS is broad and weak.[13−15] XAS at the metal $L_{2,3}$-edge excites $2p^63d^n \rightarrow 2p^53d^{n+1}$ transitions (where n is the number of d-electrons in the ground state), thereby probing the unoccupied density of d states, and offering a powerful tool for electronic structure characterization. L-edge, or 2p, XAS is sensitive to the metal valence state, crystal field strength, ligand coordination geometry, and electron−electron interactions such as 2p−3d Coulomb and exchange integrals. With the aid of ligand field multiplet (LFM) calculations, one can analyze the electronic structure fingerprint that XAS spectra provide through the simulation of spectra consistent with observations.[4,16−19]

Co L-edge XAS of five closely related POMs and a Co_3O_4 thin film that exhibit different activities for photocatalytic water oxidation are investigated. The POMs vary according to the number and position of Co sites within the POM structure, the

Received: December 12, 2014
Revised: January 23, 2015
Published: January 26, 2015

DOI: 10.1021/jp5124037
J. Phys. Chem. C 2015, 119, 4173−4179

Co valence state, the coordination geometry of oxygen ligands surrounding the Co center(s), and heteroatom identity. Of these, only the POMs with multiple Co sites within a single molecular structure are highly active water oxidation catalysts. Yin et al. reports a turnover frequency (TOF) of ≥ 5 s^{-1} for $Na_{10}[Co_4(H_2O)_2(\alpha\text{-}PW_9O_{34})_2]\cdot nH_2O$ while Lv et al. found $Na_{10}[Co_4(H_2O)_2(VW_9O_{34})_2]\cdot 35H_2O$ has a TOF of >1000 s^{-1} under conditions noted within references.[11,12] The other three POMs do not exhibit any catalytic activity. Despite the large differences in water oxidation activity within this set of POMs, the electronic structure of the Co ions could not be directly correlated with catalytic activity. However, well-defined valencies, crystal field strengths, electronic-electronic interaction parameters, and structural distortions are determined with a high degree of accuracy (e.g., ligand field parameters to within ±0.1 eV) due to the model, homogeneous POM systems. Prior Co XAS studies have been limited by the heterogeneous sample environment of Co centers. That is, Co ions may exist in a mix of substitutional and interstitial sites due to structural defects, such as oxygen and metal vacancies, or Co may phase separate to form metallic Co clusters.[3−5] The trends identified from the well-characterized POMs allow for simulation of a heterogeneous Co_3O_4 thin film. Such studies set the stage for investigating Co-based catalysts by *in situ* L-edge XAS and highlight the neccessity for X-ray techniques even more sensitive to electronic structure (e.g., resonant inelastic X-ray scattering (RIXS)), that could relate their differences in catalytic activity to ground state electronic structure.

EXPERIMENTAL SECTION

Materials Preparation and Characterization. *Co POMs.* All reagents were purchased as analytical or reagent grade and used as received. Syntheses were performed in ambient atmospheric conditions. $K_5H[Co^{II}W_{12}O_{40}]\cdot 15H_2O$,[20] $K_5[Co^{III}W_{12}O_{40}]\cdot 20H_2O$,[20] $K_6[SiCo^{II}(H_2O)W_{11}O_{39}]\cdot 10H_2O$[21] and $Na_{10}[Co_4(H_2O)_2(RW_9O_{34})_2]\cdot nH_2O$[11,12] (where R represents phosphorus (P) or vanadium(V)) were prepared based on published procedures. Using coordination geometries, number of Co's, valence states, and heteroatoms as identifiers, the POMs are labeled as T_d Co^{2+}, T_d Co^{3+}, O_h Co^{2+}, O_h $Co_4{}^{2+}P_2$, and O_h $Co_4{}^{2+}V_2$, respectively, where T_d denotes a tetrahedral geometry and O_h denotes an octahedral geometry. Representations of these POMs are shown in Figure 1. Each analogue was purified by recrystallization prior to use. Tetrahedral analogues were further purified using Dowex 50WX8 ion-exchange resin conditioned in the K^+ cycle prior to recrystallation.[22] The identities and purities of each compound were confirmed with UV−visible and infrared spectroscopy. Infrared spectra (2% by weight in KBr) were recorded on a Nicolet 6700 FT-IR spectrometer. Electronic absorption spectra were acquired using an Agilent 8453 spectrophotometer equipped with a diode-array detector and Agilent 89090A cell temperature controller unit. The UV−visible-near-infrared spectra were acquired using a Shimadzu UV-2600 spectrophotometer. UV−visible and infrared spectra are given in Supporting Information (Supporting Figures 1 and 2).

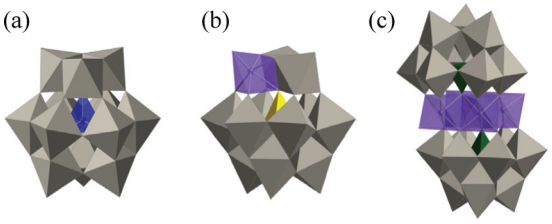

Figure 1. Polyhedral representations of POM analogues showing location and number of Co tetrahedra (blue), Co octahedra (purple), and tungstate octahedra (gray). Analogues studied include (a) T_d Co in a 2^+ or 3^+ oxidation state (b) O_h Co^{2+} with a neighboring silicon heteroatom (yellow), and (c) four O_h Co^{2+} centers in the POM core with neighboring phosphorus or vanadium heteroatoms (green).

Co_3O_4 Thin Film. Co_3O_4 films were deposited on SiO_2 substrates by DC reactive magnetron sputtering (AJA International) from a 2″ Co target with 99.95% purity at a working power of 40 W. A total pressure of 5 mTorr was used with a ratio of 20:2 sccm Ar:O_2 at a growth temperature of 600 °C. Film thickness of ∼200 nm was obtained based on a deposition rate of 0.342 Å s^{-1} calculated from the quartz crystal monitor. After deposition, the Co_3O_4 film was postannealed for 6 h at 700 °C in 1 atm O_2. Structural analysis was determined using power X-ray diffraction (XRD) from a Siemens D500 Diffractometer with Cu Kα radiation and Raman spectroscopy. The Raman spectrum was obtained from a macro-Raman system with a 488 nm Ar ion laser and triple spectrometer using a 0.6 m dispersion stage with a resolution of ∼4 cm^{-1}. XRD patterns and Raman spectrum, given in Supporting Information (Supp. Figure 3.), confirm polycrystalline Co_3O_4 thin films. These sputtered films typically have structural defects due to ∼1% Co vacancies and a p-doping of $\sim 10^{20}$ cm^{-3}.[23]

X-ray Absorption Spectroscopy. XAS measurement: Co POM crystals were spread directly onto conductive copper or carbon-based adhesive tape or pressed onto indium foil and affixed to a specially designed beamline sample holder for X-ray analysis. The Co_3O_4 thin film on SiO_2 was also attached to the beamline sample holder with adhesive tape. A drop of conductive silver paste at the sample edge and holder supported conductivity across assembly. A cobalt foil reference was used for energy calibration.[24]

XAS experiments were performed at beamlines 7.0.1 and 8.0.1 at the Advanced Light Source (ALS) at Lawrence Berkeley National Laboratory. The X-ray absorption process was measured using total electron yield (TEY) and total fluorescence yield (TFY) detection modes. The TEY signal originates from the cascade of secondary electrons created upon relaxation of the excited core-level electron, while TFY arises from the emission of a fluorescent X-ray photon upon relaxation. TEY was collected by measuring the sample drain current, and the TFY signal was acquired using a channeltron detector equipped with a negatively biased grid to repel electrons ejected from the sample. The inelastic mean free path of electrons and photons determines the experimental probing depth, rendering TEY more surface sensitive and TFY more bulk sensitive. LFM calculations are more representative of TEY detected spectra, since saturation effects can complicate TFY spectra as suggested previously.[25,26] Therefore, TEY spectra are primarily reported, and only TFY is used when bulk sensitivity is required. The sample was positioned at ∼45° to the incident X-ray beam with a ∼30° angle between X-ray beam and channeltron detector. The analysis chamber was kept lower than 2.0×10^{-8} Torr during data acquisition. All spectra were normalized by I_0, the incident X-ray beam current as detected by gold foil upstream from the sample analysis chamber. Data was collected using beamline specific software and processed

DOI: 10.1021/jp5124037
J. Phys. Chem. C 2015, 119, 4173−4179

using custom panels in the Wavemetrics, Inc. Igor Pro 6.22A software.

Ligand Field Multiplet Calculations. LFM theory was used to simulate experimental Co $L_{2,3}$-edge XAS spectra. The 2p XAS process corresponds to $2p^63d^7 \rightarrow 2p^53d^8$ and $2p^63d^6 \rightarrow 2p^53d^7$ transitions for Co^{2+} and Co^{3+}, respectively. Spectra were calculated with the aid of CTM4XAS and CTM4RIXS,[27] a freeware interface version of the Cowan–Butler–Thole code as developed by Thole et al.[28−30] XAS spectra were calculated to reproduce experimental TEY spectra while a linear combination of 25% XAS and 75% RIXS spectra were used to reproduce experimental TFY spectra. Simulated XAS spectra take into account atomic multiplet effects, which determine how the molecular nature of the compound affects the XAS spectra. Atomic multiplet effects are included by a reduction of the Slater integrals from their atomic values, introducing a ligand field, and adding charge transfer processes as needed. The Slater integrals represent the Coulomb repulsion between the core and 3d electrons $\langle 2p3dl1/r_{1,2}|2p3d\rangle$ (F_{pd}), the Coulomb repulsion of the 3d electrons $\langle 3d3dl1/r_{1,2}|3d3d\rangle$ (F_{dd}) and the exchange $\langle 2p3dl1/r_{1,2}|3d2p\rangle$ (G_{pd}) integrals in the presence of a core hole. Atomic values were used for core spin–orbit coupling, ξ_{2p}, but were reduced from atomic values for the valence spin–orbit coupling, ξ_{3d}, depending on the spin of the valence electrons. The ligand field is parametrized by 10*Dq* values, ligand field symmetry, and axial distortion, *Ds*. To reproduce experimental spectra, it was unnecessary to explicitly include charge transfer states; rather, such effects were implicitly accounted for by reduction of the Slater integrals. As the calculations do not result in an absolute energy value, simulated spectra are shifted to align with experimental spectra. Calculations are done at 300 K, and the resulting spectra are broadened to account for core-hole lifetimes and experimental resolutions, represented by Lorentzian, Γ, and Gaussian, *G*, functions, respectively. For this, we use half-width half-maximum values of $\Gamma(L_3)$ = 0.2 eV, $\Gamma(L_2)$ = 0.4 eV, and *G* = 0.15 eV.

RESULTS AND DISCUSSION

Experimental Co L-edge XAS spectra for 5 POM analogues (representations in Figure 1) are shown in Figure 2; analogues vary according to the number and position of Co sites within the POM structure (1 or 4 cobalt(s)), the Co valence state (2^+ or 3^+), coordinating geometry (O_h or T_d), and the identity of the heteroatom (e.g., Si, P, or V). The Co L-edge is split into two peaks due to core-level spin–orbit coupling (ξ_{2p}): the lower energy L_3 peak ($2p_{3/2} \rightarrow 3d$) and higher energy L_2 peak ($2p_{1/2} \rightarrow 3d$). The splitting is set by the atomic value of ξ_{2p} for all the compounds studied. It is the L_3 edge, shown in Figure 2, that gets split prominently by electron–electron interactions that give rise to a multiplet structure.

Furthermore, the multiplet structure of the L_3 edge depends distinctly on the coordination of the Co center. For example, the TEY spectrum of O_h Co^{2+} has a low energy shoulder at 776.4 eV not present in the T_d Co^{2+} case. Note from the similarity of the L_3 structure that L-edge XAS is not sensitive enough to detect differences in the electronic structure due to the heteroatom (P or V) or to the number of Co sites (1 or 4) within the POM structure. Rather, the Co valence state and coordination geometry define the multiplet structure of L_3. Figure 3 shows LFM simulated spectra of Co^{2+} and Co^{3+} in both O_h and T_d environments compared with experimental L_3 XAS spectra of a Co_3O_4 thin film (Figure 3a), O_h Co^{2+} POM

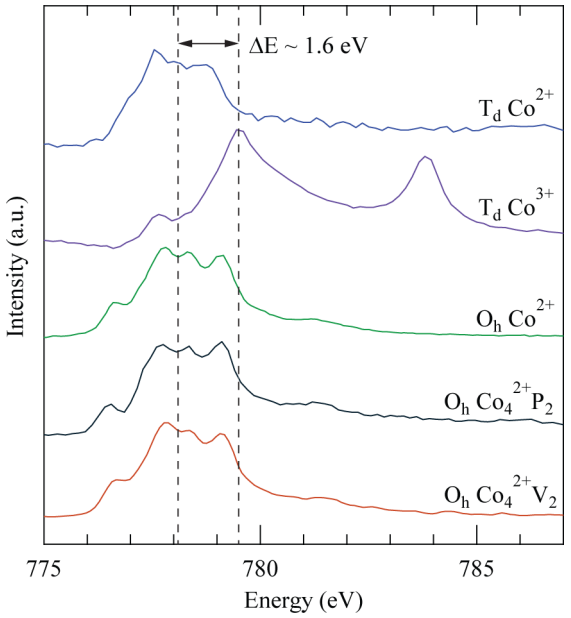

Figure 2. Experimental Co $2p_{3/2}$ XAS spectra of POM analogues for T_d Co^{2+}, T_d Co^{3+}, O_h Co^{2+}, O_h $Co_4{}^{2+}P_2$, and O_h $Co_4{}^{2+}V_2$. All spectra are based on TEY detection except for the one in part d for T_d Co^{3+} which is from TFY detection. Because of the highly oxidizing T_d Co^{3+} POM oxidizing the surface, TEY was not representative of the bulk structure.

(Figure 3b), T_d Co^{2+} POM (Figure 3c), and T_d Co^{3+} POM (Figure 3d). The parameters varied, namely the crystal field parameters, 10*Dq* and *Ds*, the Slater integral reduction (SIR), and the valence spin orbit coupling reduction (VSOCR) are shown in Table 1. The Co $2p_{3/2}$ XAS spectrum of a reference bulk CoO compound is included in Supporting Information (Supporting Figure 4). There, it is compared directly with the Co $2p_{3/2}$ XAS spectrum of O_h Co^{2+} POM and the LFM simulated spectrum.

For all but one of the samples, TEY spectra are collected; however, for T_d Co^{3+} POM, reduction of the surface Co centers to Co^{2+} necessitated collection by TFY. Comparison of the TEY and TFY spectra for the T_d Co^{3+} POM are provided in Supporting Information (Supporting Figure 5).

Valence State. The valence state of the Co ion is determined experimentally and used as an input into the LFM calculations below. The effect of the valence state on the absorption energy cannot be determined theoretically with precision using ligand field models because screening effects are not included correctly. The valence state is determined experimentally by the approximate peak center of the L_3 edge for two Co ions in the same coordination geometry. As shown in Figure 2, T_d Co^{3+} occurs ~1.6 eV higher in energy than T_d Co^{2+}. This is consistent with previous reports on energy shift per valence state change found for 3d transition metal oxides.[31,32] To provide another example, the experimental Co 2p XAS of a Co_3O_4 thin film is shown in Figure 3a. Cobalt oxide has a spinel structure consisting of Co^{2+} and Co^{3+} in T_d and O_h sites, respectively. The pronounced L_3 doublet peak structure is assigned to these oxidation states with Co^{2+} at 777.7 eV and Co^{3+} at 779.4 eV; this again gives a 1.7 eV energy shift with valence state.

Ligand Field and Structural Distortions. The values of ligand field parameter, 10*Dq*, applied to the calculated spectra shown in Figure 3 are given in Table 1. A negative 10*Dq* value

DOI: 10.1021/jp5124037
J. Phys. Chem. C 2015, 119, 4173−4179

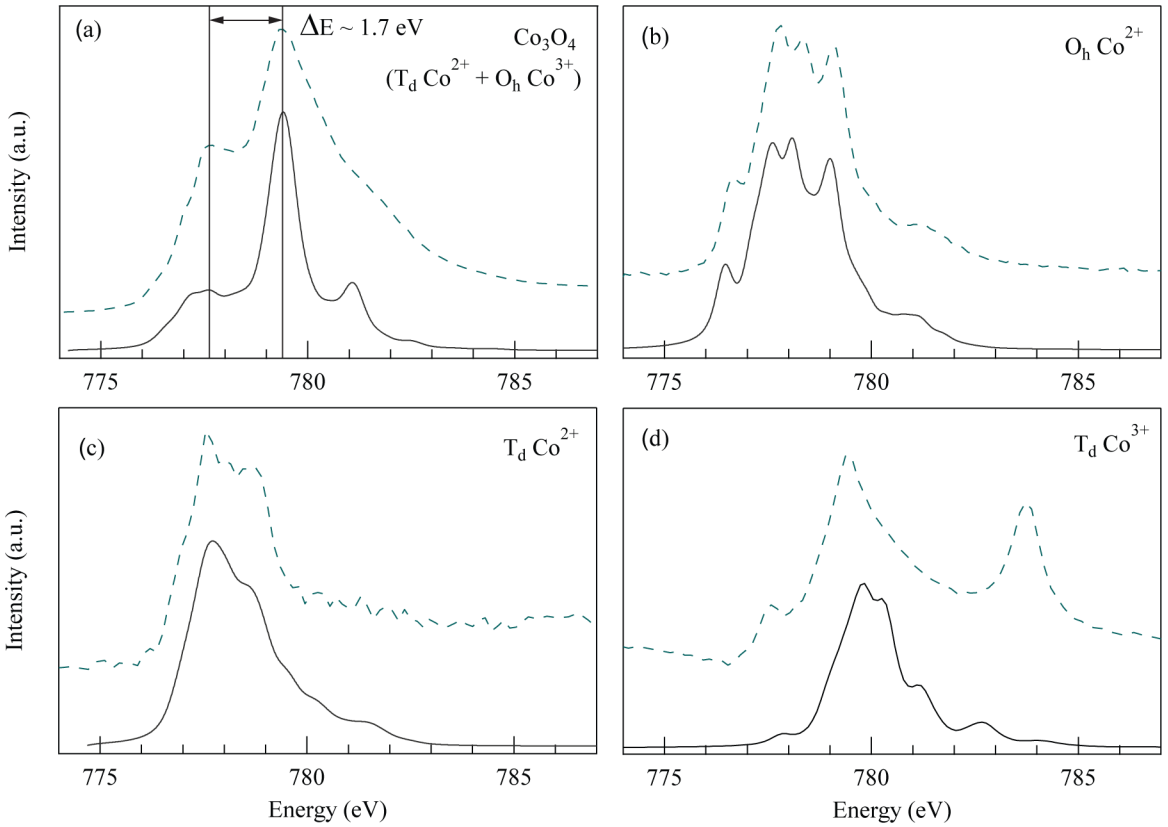

Figure 3. Cobalt $2p_{3/2}$ XAS spectra of (a) Co_3O_4 thin film (dashed line) and LFM calculated spectrum (solid line). The simulated spectrum is created by a stoichiometric combination of high-spin ($10Dq$ = 0.75 eV) T_d Co^{2+} and low-spin ($10Dq$ = 1.8 eV) O_h Co^{3+} spectra, each normalized to the integrated intensity of allowed transitions related to the number of 3d holes in the ground state. Experimental (dashed line) and LFM calculated (solid line) cobalt $2p_{3/2}$ XAS spectra of (b) O_h Co^{2+} POM, (c) T_d Co^{2+} POM, and (d) T_d Co^{3+} POM. All spectra are based on TEY detection except for the one in part d for T_d Co^{3+}, which is based on TFY detection. Because of the highly oxidizing T_d Co^{3+} POM oxidizing the surface, TEY was not representative of the bulk structure.

Table 1. Electronic Structure Parameters Used for Fitting L-Edge Absorption Spectra for Select Absorbers

absorber	final state $10Dq$ (eV)	SIR[a] (%) (F_{dd}, F_{pd}, G_{pd})	VSOCR[b] (%)
T_d Co^{2+} (POM)	−0.7 ± 0.1	0.9 ± 0.05	1.0
T_d Co^{3+} (POM)	−0.8	0.8	0.0
O_h Co^{2+} (POM)	0.8 ± 0.1 ($4Ds$ = 0.16)	0.9 ± 0.05	0.7
T_d Co^{2+} (Co_3O_4)	−0.75	0.9	1.0
O_h Co^{3+} (Co_3O_4)	1.8	0.7	1.0

[a]Slater integral reduction. [b]Valence spin−orbit coupling reduction.

for the T_d structures indicates d-orbital splitting, with a lower energy (e) and higher energy (t_2) set, that is reversed from the O_h case (where t_{2g} is lower and e_g is higher). The value of $10Dq$ increases for O_h structures relative to T_d due to the larger number of ligand atoms (6 versus 4), though the increase is mitigated by the longer metal−oxygen distances in an O_h geometry that also reduces the $10Dq$. An increase in metal oxidation state also indicates a stronger bond with the oxygen ligands, and therefore increases $10Dq$, reflected in the larger value of $10Dq$ = 1.8 eV for O_h Co^{3+} in Co_3O_4 vs $10Dq$ = 0.8 eV O_h Co^{2+} POM. These markedly different ligand field splittings result in a low-spin electron configuration for Co^{3+} in Co_3O_4 and a high-spin configuration for the O_h Co^{2+} POM.

In XAS experiments, it is the final state $10Dq$ value that dictates spectral shape. The magnitude of the X-ray $10Dq$ is routinely found to be less than the UV−vis $10Dq$, which measures the ground state $10Dq$.[31] The difference is due to the presence of a core hole in the final state for the X-ray absorption process, which is understood to increase localization of metal d orbitals and thus decrease the magnitude of the energy splitting. For example, in the O_h Co^{2+} case, the optical $10Dq$ value is 1.0 eV while the X-ray $10Dq$ was determined to be 0.8 eV. Optical $10Dq$ values were calculated using the Tanabe-Sugano diagram.[33] The UV−vis-near-infrared spectra for select POM analogues are included in Supporting Information (Supporting Figure 2).

The inclusion of a small axial distortion, Ds = 0.04 eV, was necessary to reproduce the shoulder (781.3 eV) on the high energy side of L_3 for the O_h Co^{2+} ion. This distortion reduces the symmetry from O_h to D_{4h} and is consistent with X-ray crystallography studies of POM structure.[34,35] The Ds parameter corresponds to an elongation of the z-axis, yielding an energy difference between the d_{z^2} and $d_{x^2-y^2}$ orbital of $4Ds$, or 0.16 eV. In agreement with previous X-ray structural studies, it was not necessary to introduce a distortion for the T_d Co^{2+} POM.[36,37]

While the O_h Co^{2+} POM and the T_d Co^{2+} POM agree very well with their simulated spectrum, deviations are visible in the T_d Co^{3+} POM and thin film Co_3O_4. In particular, for the T_d Co^{3+} POM the shoulder at 778 eV is more pronounced in the experiment. Potentially, this can be attributed to the reduction of surface Co atoms that dominate the TEY spectrum, and appear in the bulk TFY spectrum. The shoulder is at the same

DOI: 10.1021/jp5124037
J. Phys. Chem. C 2015, 119, 4173−4179

energy as the sharp peak in the multiplet structure of the reduced TEY spectrum shown in Supporting Figure 5. While the TEY spectrum are clearly indicative of a reduced Co center, they are not equivalent to the T_d Co^{2+} POM. Therefore, a simulated addition of two Co T_d centers with different oxidation states cannot be used to provide a better agreement and thereby quantify the extent of Co metal center reduction. The peak located at ~784 eV consistently appears in the TFY spectra of the POMs and not the TEY. Others have also observed this fluorescent peak at both the ALS and European Synchrotron Radiation Facility and previously assigned it as originating from charge transfer satellites or cobalt-acetate residues.[17,38] Recent experiments show this peak also appears prominently in systems with no cobalt, ruling out a cobalt-sample related assignment.

For thin film Co_3O_4, the contribution of T_d Co^{2+} to the simulation, when included with a stoichiometric ratio of Co^{2+} to Co^{3+}, is smaller than suggested by experiment. Deviations in the Co_3O_4 thin film likely involve site-mixing due to the Co vacancies that introduce structural distortions, where O_h Co^{2+} and T_d Co^{3+} states also exist.[39,40] Indeed the greater contribution to the low energy peak at 777.7 eV could be due to mixing of O_h/T_d Co contributions for both the 2^+ and 3^+ valence states, since according to the homogeneous POMs, these two coordination geometries are centered at approximately the same energy for a given valence state (e.g., Figure 3b,c). However, even a simulation considering this mixing does not fully account for the observed experimental spectrum, and suggests that other effects should be included to describe the heterogeneity of the thin film.

Ligand field 10Dq values are further justified by showing changes in calculated spectra as a function of this parameter (Figure 4) and compared with experimental spectra for O_h Co^{2+} POM and T_d Co^{2+} POM. 10Dq is varied from 0.5−1.4 eV in 0.3 eV steps while the remaining parameter values (discussed below) are kept constant. In the O_h Co^{2+} case, large changes in peak shape arise due to the transition from the high spin to low spin configuration. From Figure 4a, one can see that a 10Dq value around 0.8 eV is consistent with the experimental spectrum of O_h Co^{2+}. Small step sizes of 0.1 eV around this value produce appreciable changes in the spectrum (Figure 4c), such that 10Dq = 0.8 eV to within ±0.1 eV can be reported. Similarly, 10Dq = −0.7 eV to within ±0.1 eV agrees with the experimental T_d Co^{2+} (Figure 4b,d).

Electron−Electron Interactions: Slater Integral Reduction and Valence Spin−Orbit. As shown in Table 1, for all the compounds studied a reduction of the Slater integrals is required, with 90% of the atomic value for Co^{2+} absorbers and 70−80% for Co^{3+} absorbers. Reducing the Slater parameters can be understood as simulating an increased d-electron delocalization, or covalency, that occurs in going from a free ion to a complex; this is commonly described as the nephelauxetic effect in transition metal complexes.[41,42] The degree of covalency, and thus SIR, becomes more significant as the oxidation state of the metal center increases. As above with 10Dq, further justification for SIR values is provided by varying them from 50% - 110% in 20% steps (Figure 5) for the O_h Co^{2+} and T_d Co^{2+} cases. In general, as the reduction increases and the separation between atomic multiplet states becomes smaller, the L_3 peak splitting decreases and the edge becomes centered around a single distinct peak. Judging by the spectra in Figure 5a,b, in both cases a SIR value of around 90% is a reasonable choice for the 2^+ valence state. Slater integrals

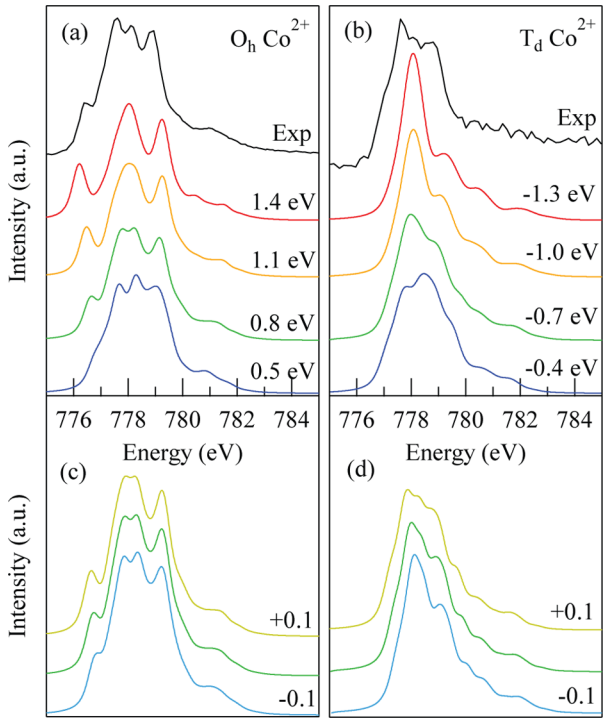

Figure 4. (a) O_h and (b) T_d Co^{2+} spectra calculated at a series of crystal field splitting parameters (10Dq). (c and d) Spectra for small step sizes with 10Dq values ±1 eV from 0.8 and −0.7 eV, respectively. All other electronic structure parameters are held constant.

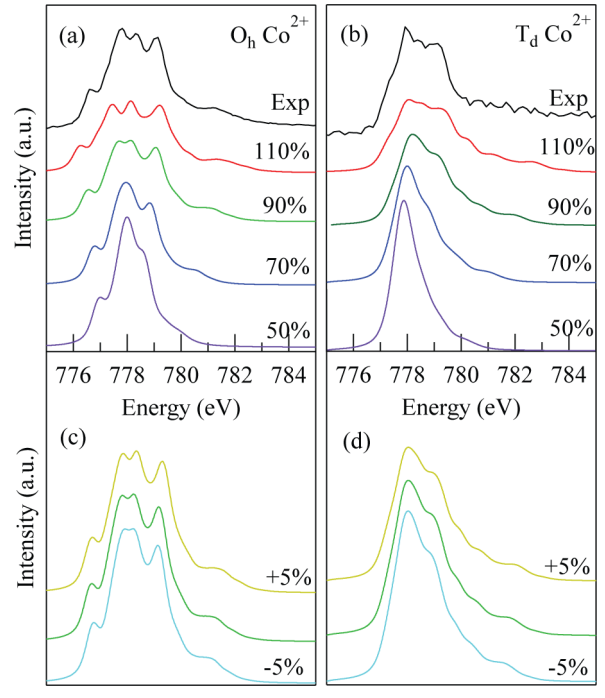

Figure 5. (a) O_h and (b) T_d Co^{2+} spectra calculated at a series of Slater integral reduction values (% F_{dd}, F_{pd}, G_{pd}). (c and d) Spectra for small step sizes with Slater integral reduction values ±5% from 90%. All other electronic structure parameters are held constant.

reduced by ±5% around 90% provide an error bar for visual inspection (Figure 5c,d).

The last parameter to be discussed is the valence spin−orbit coupling reduction, or VSOCR. Reduction of the 3d spin−orbit

DOI: 10.1021/jp5124037
J. Phys. Chem. C 2015, 119, 4173−4179

coupling from its atomic value is due primarily to ligand field effects that change the d-orbital occupation, but can also come from delocalization effects. In cases such as T_d Co^{2+} and low-spin O_h Co^{3+}, where the ground state electronic configuration ($e^4t_2^3$ and t_{2g}^6, respectively) has A symmetry, there is no difference in the spin−orbit coupling from the atomic state and this parameter can be left the same. However, the high-spin O_h Co^{2+} case (Figure 3b) requires a reduction to 70% of the atomic value, due to a half-filled t_{2g} orbital that does change the d-orbital occupation. This is consistent with previous values used to calculate spectra for CoO nanocrystals.[16] In contrast, a full quenching (0%) of the atomic value is necessary for T_d Co^{3+} due to a change in the orbital occupation of the e orbitals.[43,44]

CONCLUSIONS

We have characterized the electronic structure of Co centers in a set of nanoscale Co POMs and a Co_3O_4 thin film using L-edge XAS. Spectra were analyzed by LFM theory to obtain the valence state, the strength of the ligand field through 10*Dq*, the effect of structural distortions through *Ds*, and the degree of covalency through reduction of the Slater integrals. Together, these parameters depict the electronic structure of the unoccupied d-electron states of Co^{2+} and Co^{3+} in O_h and T_d environments within well-defined model systems. The work demonstrates the straightforward use of LFM theory and provides a benchmark for the many Co containing photocatalysts currently being investigated. While ab initio calculations of the L-edge are beyond the scope of current computational techniques, the multiplet structure of the L_3 edge provides a fingerprint that differentiates the ground state electronic structure of Co-based catalysts. We also find that L-edge XAS is not sensitive enough to detect differences in electronic structure due to multiple Co atoms in similar local environments, or to heteroatoms in the Co atom's vicinity. However, the availability of these other Co sites in the POMs as well as the heteroatoms do significantly affect their catalytic activity. Therefore, the work also shows that even more sensitive X-ray techniques, such as RIXS, should be employed to detail the differences in the ground state electronic structure that could affect reactivity.

ASSOCIATED CONTENT

Supporting Information

Compound characterization data, IR and UV−vis electronic absorption spectra of five Co POMs. UV−vis−near-infrared electronic absorption spectra of select Co POMs, Raman spectrum and XRD patterns of a Co_3O_4 thin film, Co $2p_{3/2}$ XAS spectrum of a reference bulk CoO compound compared with O_h Co^{2+} POM and LFM simulated spectra, and TEY and TFY Co $2p_{3/2}$ XAS spectra for T_d Co^{3+} POM. This material is available free of charge via the Internet at http://pubs.acs.org

AUTHOR INFORMATION

Corresponding Author

*(T.C.) E-mail: tanjacuk@berkeley.edu.

Author Contributions

‖Contributed equally to this work

Notes

The authors declare no competing financial interest.

ACKNOWLEDGMENTS

This material is based on research sponsored by the Air Force Research Laboratory, under agreement number FA9550-12-1-0337. H.Q.D. was supported by the National Science Foundation Graduate Student Fellowship. We thank the Frances Hellman Lab in the Physics Department at University of California—Berkeley for the use of the sputtering system and the Joel Ager Lab in the Materials Sciences Division at Lawrence Berkeley National Laboratory and the Material Sciences Division X-ray Diffraction facility for use of characterization equipment. Dr. Jinghua Guo, Dr. Wanli Yang, Mr. Wei-Cheng Wang, Mr. Hui Zhang, and Ms. Ruimin Qiao are gratefully acknowledged for their help at the Advanced Light Source.

REFERENCES

(1) Liu, X.-C.; Shi, E.-W.; Chen, Z.-Z.; Zhang, T.; Zhang, Y.; Chen, B.-Y.; Huang, W.; Liu, X.; Song, L.-X. Effect of Donor Localization on the Magnetic Properties of Zn-Co-O System. *Appl. Phys. Lett.* **2008**, *92*, 042502−3.

(2) Chang, G.; Kurmaev, E.; Boukhvalov, D.; Finkelstein, L.; Colis, S.; Pedersen, T.; Moewes, A.; Dinia, A. Effect of Co and O Defects on the Magnetism in Co-Doped ZnO: Experiment and Theory. *Phys. Rev. B* **2007**, *75*, 195215−7.

(3) Lee, Y.; de Jong, M.; Jansen, R. Magnetism and Heterogeneity of Co in Anatase Co:TiO_2 Magnetic Semiconductor. *Appl. Phys. Lett.* **2010**, *96*, 082506−3.

(4) Lee, Y.; de Jong, M.; van der Wiel, W. Electronic Structure of Co^{2+} Ions in Anatase Co:TiO_2 in Relation to Heterogeneity and Structural Defects. *Phys. Rev. B* **2011**, *83*, 134404−5.

(5) Lussier, A.; Dvorak, J.; Idzerda, Y.; Shinde, S.; Ogale, S.; Venkatesan, T. XAS Characterization of Growth Parameter Effects for Pulsed Laser Deposited $Co_xTi_{1-x}O_{2-\delta}$ Films. *Phys. Scr.* **2005**, *T115*, 623−625.

(6) Whittingham, M. Lithium Batteries and Cathode Materials. *Chem. Rev.* **2004**, *104*, 4271−4302.

(7) Etacheri, V.; Marom, R.; Elazari, R.; Salitra, G.; Aurbach, D. Challenges in the Development of Advanced Li-Ion Batteries: A Review. *Energy Environ. Sci.* **2011**, *4*, 3243−3262.

(8) Jiao, F.; Frei, H. Nanostructured Cobalt Oxide Clusters in Mesoporous Silica as Efficient Oxygen-Evolving Catalysts. *Angew. Chem., Int. Ed.* **2009**, *48*, 1841−1844.

(9) Zhang, M.; de Respinis, M.; Frei, H. Time-Resolved Observations of Water Oxidation Intermediates on a Cobalt Oxide Nanoparticle Catalyst. *Nat. Chem.* **2014**, *6*, 362−367.

(10) Kanan, M.; Nocera, D. In Situ Formation of an Oxygen-Evolving Catalysts in Neutral Water Containing Phosphate and Co^{2+}. *Science* **2008**, *321*, 1072−1075.

(11) Yin, Q.; Tan, J.; Besson, C.; Geletii, Y.; Musaev, D.; Kuznetsov, A.; Luo, Z.; Hardcastle, K.; Hill, C. A Fast Soluble Carbon-Free Molecular Water Oxidation Catalyst Based on Abundant Metals. *Science* **2010**, *328*, 342−345.

(12) Lv, H.; Song, J.; Geletii, Y.; Vickers, J.; Sumliner, J.; Musaev, D.; Kögerler, P.; Zhuk, P.; Bacsa, J.; Zhu, G.; Hill, C. An Exceptionally Fast Homogeneous Carbon-Free Cobalt-Based Water Oxidation Catalyst. *J. Am. Chem. Soc.* **2014**, *136*, 9268−9271.

(13) Kanan, M.; Yano, J.; Surendranath, Y.; Dincă, M.; Yachandra, V.; Nocera, D. Structure and Valency of a Cobalt-Phosphate Water Oxidation Catalyst Determined by In Situ X-ray Spectroscopy. *J. Am. Chem. Soc.* **2010**, *132*, 13692−13701.

(14) Schiwon, R.; Klingan, K.; Dau, H.; Limberg, C. Shining Light on Integrity of a Tetracobalt-Polyoxometalate Water Oxidation Catalyst by X-ray Spectroscopy Before and After Catalysis. *Chem. Commun.* **2014**, *50*, 100−102.

(15) Ohlin, C.; Harley, S.; McAlpin, J.; Hocking, R.; Mercado, B.; Johnson, R.; Villa, E.; Fidler, M.; Olmstead, M.; Spiccia, L.; Britt, R.; Casey, W. Rates of Water Exchange for Two Cobalt(II) Hetero-

DOI: 10.1021/jp5124037
J. Phys. Chem. C 2015, 119, 4173−4179

polyoxotungstate Compounds in Aqueous Solution. *Chem.—Eur. J.* **2011**, *17*, 4408−4417.
(16) van Schooneveld, M.; Kurian, R.; Juhin, A.; Zhou, K.; Schlappa, J.; Strocov, V.; Schmitt, T.; de Groot, F. Electronic Structure of CoO Nanocrystals and a Single Crystal Probed by Resonant X-ray Emission Spectroscopy. *J. Phys. Chem. C* **2012**, *116*, 15218−15230.
(17) Liu, H.; Guo, J.; Yin, Y.; Augustsson, A.; Dong, C.; Nordgren, J.; Chang, C.; Alivisatos, P.; Thornton, G.; Ogletree, D.; et al. Electronic Structure of Cobalt Nanocrystals Suspended in Liquid. *Nano Lett.* **2007**, *7*, 1919−1922.
(18) Bonhommeau, S.; Pontius, N.; Cobo, S.; Salmon, L.; de Groot, F.; Molnar, G.; Bousseksou, A.; Durr, H.; Eberhardt, W. Metal-to-Ligand and Ligand-to-Metal Charge Transfer in Thin Films of Prussian Blue Analogues Investigated by X-ray Absorption Spectroscopy. *Phys. Chem. Chem. Phys.* **2008**, *10*, 5882−5889.
(19) Cartier dit Moulin, C.; Villain, F.; Bleuzen, A.; Arrio, M.-A.; Sainctavit, P.; Lomenech, C.; Escax, V.; Baudelet, F.; Dartyge, E.; Gallet, J.-J.; et al. Photoinduced Ferrimagnetic Systems in Prussian Blue Analogues $C^{I}_{x}Co_4[Fe(CN)_6]_y$ (C_I = Alkali Cation). 2. X-ray Absorption Spectroscopy of the Metastable State. *J. Am. Chem. Soc.* **2000**, *122*, 6653−6658.
(20) Glass, E.; Fielden, J.; Kaledin, A.; Musaev, D.; Lian, T.; Hill, C. Extending Metal-to-Polyoxometalate Charge Transfer Lifetimes: The Effect of Heterometal Location. *Chem.—Eur. J.* **2014**, *20*, 4297−4307.
(21) Müller, A.; Dloczik, L.; Diemann, E.; Pope, M. A Cyclic Voltammetric Study of Mangano(II)undecatungstosilicate: An Illustrative Example of the Reduction, Protonation and Disproportionation Pathways of Transition Metal Substituted Heteropolytungstates in Aqueous Solution. *Inorg. Chim. Acta* **1997**, *257*, 231−239.
(22) Simmons, V. Heteropoly Tungstocobaltoates and Tungstocobaltiates Based on CoO_4 Tetrahedra: Magnetic Properties, Spectra, Chemistry, and Structures. Ph.D. Dissertation, Boston University: Boston, 1953.
(23) Schumacher, L.; Holzhueter, I.; Hill, I.; Dignam, M. Semiconducting and Electrocatalytic Properties of Sputtered Cobalt Oxide Films. *Electrochim. Acta* **1990**, *35*, 975−987.
(24) Fuggle, J.; Mårtensson, N. Core-Level Binding Energies in Metals. *J. Electron Spectrosc. Relat. Phenom.* **1980**, *21*, 275−281.
(25) Eisebitt, S.; Böske, T.; Rubensson, J.-E.; Eberhardt, W. Determination of Absorption Coefficients for Concentrated Samples by Fluorescence Detection. *Phys. Rev. B* **1993**, *47*, 14103−14109.
(26) Tröger, L.; Arvanitis, D.; Baberschke, K.; Michaelis, H.; Grimm, U.; Zschech, E. Full Correction of the Self-Absorption in Soft-Fluorescence Extended X-ray-Absorption Fine Structure. *Phys. Rev. B* **1992**, *46*, 3283−3289.
(27) Stavitski, E.; de Groot, F. The CTM4XAS Program for EELS and XAS Spectral Shape Analysis of Transition Metal L Edges. *Micron* **2010**, *41*, 687−694.
(28) de Groot, F.; Fuggle, J.; Thole, B.; Sawatzky, G. 2p X-ray Absorption of 3d Transition-Metal Compounds: An Atomic Multiplet Description Including the Crystal Field. *Phys. Rev. B* **1990**, *42*, 5459−5468.
(29) Cowan, R. Theoretical Calculations of Atomic Spectra Using Digital Computers. *J. Opt. Soc. Am.* **1968**, *58*, 808−818.
(30) Thole, B.; Van Der Laan, G.; Butler, P. Spin-Mixed Ground State of Fe Phthalocynanine and the Temperature-Dependent Branching Ratio in X-ray Absorption Spectroscopy. *Chem. Phys. Lett.* **1988**, *149*, 295−299.
(31) Cramer, S.; de Groot, F.; Ma, Y.; Chen, C.; Sette, F.; Kipke, C.; Eichhorn, D.; Chan, M.; Armstrong, W. Ligand Field Strengths and Oxidation States from Manganese L-Edge Spectroscopy. *J. Am. Chem. Soc.* **1991**, *113*, 7937−7940.
(32) Heijboer, W.; et al. In-Situ Soft X-ray Absorption of Over-Exchanged Fe/ZSM5. *J. Phys. Chem. B* **2003**, *107*, 13069−13075.
(33) Tanabe, Y.; Sugano, S. On the Absorption Spectra of Complex Ions II. *J. Phys. Soc. Jpn.* **1954**, *9*, 766−779.
(34) Dawson, B. The Structure of the 9(18)-Heteropoly Anion in Potassium 9(18)-Tungstophosphate, $K_6(P_2W_{18}O_{62})\cdot 14H_2O$. *Acta Crystallogr.* **1953**, *6*, 113−126.
(35) Kobayashi, A.; Sasaki, Y. The Crystal Structure of α-Barium 12-Tungstosilicate, α-$Ba_2SiW_{12}O_{40}\cdot 16H_2O$. *Bull. Chem. Soc. Jpn.* **1975**, *48*, 885−888.
(36) Nolan, A.; Allen, C.; Burns, R.; Craig, D.; Lawrance, G. X-ray Structural Studies of $K_6[Co^{II}W_{12}O_{40}]16H_2O$ and $K_5[Co^{III}W_{12}O_{40}]$-$16H_2O$ and Structural Trends Along the $[XW_{12}O_{40}]^{n-}$ Series, where X = P^{V}, Si^{IV}, Co^{III} and Co^{II}. *Aust. J. Chem.* **2000**, *53*, 59−66.
(37) Brown, G.; Noe-Spirlet, M.-R.; Busing, W.; Levy, H. Dodecatungstophosphoric Acid Hexahydrate, $(H_5O_2^{+})_3(PW_{12}O_{40}^{3-})$. The True Structure of Keggin's 'Pentahydrate' from Single-Crystal X-ray and Neutron Diffraction Data. *Acta. Crystallogr., Sect. B* **1977**, *33*, 1038−1046.
(38) Flipse, C.; Rouwelaar, C.; de Groot, F. Magnetic Properties of CoO Nanoparticles. *Eur. Phys. J. D* **1999**, *9*, 479−481.
(39) Pattrick, R.; Van Der Laan, G.; Henderson, M.; Kuiper, P.; Dudzik, E.; Vaughan, D. Cation Site Occupancy in Spinel Ferrites Studied by X-ray Magnetic Circular Dichroism: Developing a Method for Mineralogists. *Eur. J. Mineral.* **2002**, *14*, 1095−1102.
(40) Tuxen, A.; Carenco, S.; Chintapalli, M.; Chuang, C.-H.; Escudero, C.; Pach, E.; Jiang, P.; Borondics, F.; Beberwyck, B.; Alivisatos, A.; et al. Size-Dependent Dissociation of Carbon Monoxide on Cobalt Nanoparticles. *J. Am. Chem. Soc.* **2013**, *135*, 2273−2278.
(41) de Groot, F.; Hu, Z.; Lopez, M.; Kaindl, G.; Guillot, F.; Tronc, M. Differences Between L_3 and L_2 X-ray Absorption Spectra of Transition Metal Compounds. *J. Chem. Phys.* **1994**, *101*, 6570−6576.
(42) Tchougréeff, A.; Dronskowski, R. Nephelauxetic Effect Revisited. *Int. J. Quantum Chem.* **2009**, *109*, 2606−2621.
(43) Sugano, S.; Tanabe, Y.; Kamimura, H. *Multiplets of Transition-Metal Ions in Crystals*; Academic Press: New York, 1970.
(44) Griffith, J. *The Theory of Transition-Metal Ions*; Cambridge University Press: Cambridge, U.K., 2009.

DOI: 10.1021/jp5124037
J. Phys. Chem. C 2015, 119, 4173−4179